J. Solid Mech. 2025; 17(04): Article 13

Journal of Solid Mechanics

https:/doi.org/10.57647/jsm.2025.1704.13

Research Article

Length Scale Dependency of Micropolar Equations of Elasticity in Hollow Cylinder Subjected to Mechanical Load

Ameer Khalaf Ali, Mohsen Jabbari*, Seyed Mahdi Khorsandijou

Department of Mechanical Engineering, ST.C., Islamic Azad University, Tehran, Iran

***Corresponding author:** m_jabbari@azad.ac.ir

Article History:

Received:
17 October 2025

Revised:
20 November 2025

Accepted:
31 December 2025

Published in Issue:
31 December 2025

Abstract

This paper performs a numerical analysis of the stress behavior of a hollow cylinder within the framework of micropolar elasticity, taking explicitly into account length-scale effects. The governing field equations are established in polar coordinates, where size dependence is captured through characteristic material length parameters and the formulation is given in terms of stress functions. The resulting boundary value problem is then solved by using the Generalized Differential Quadrature (GDQ) technique. The obtained numerical results clearly show a strong dependency of the stress response from the material length parameter. Indeed, increasing the latter from l=0 the value corresponding to the classical elasticity model-to the considered micrometer scale value, the maximum values of radial and circumferential stresses decrease by about 46% and 45%, respectively, whereas the maximum value of couple stress $m_{r\theta}$ decreases by about 30%. These findings are particularly relevant for micro-scale engineering applications such as MEMS devices and biomedical implants, where component dimensions approach the material's micro-structural scale and classical elasticity proves inadequate. Furthermore, the pronounced size effects observed at the inner radius where stress gradients are highest highlight the critical need for micropolar theory in accurate stress analysis of microscale cylindrical structures. This work provides a foundation for future research on functionally graded micropolar materials and establishes GDQ as an efficient computational tool for capturing intricate size-effects in advanced micro-structured components.

Keywords: Micropolar Elasticity, Generalized Differential Quadrature Method (GDQM), Length Scale Parameter, Mechanical boundary conditions

Cite this article: Ameer, K. A., Jabbari, M., Khorsandijou, S. M., (2025). Length Scale Dependency of Micropolar equations of Elasticity in hollow cylinder Subjected to Mechanical Load, *Journal of Solid Mechanics,* 17(04): Article 13. https:/doi.org/10.57647/jsm.2025.1704.13

1. Introduction

Functionally Hollow cylindrical structures are essential elements in a wide array of engineering applications, including pressure vessels and piping systems within the energy sector, as well as structural components in aerospace and mechanical engineering. The precise forecasting of their mechanical performance under diverse loading conditions is crucial for maintaining structural integrity, reliability, and optimal design.

For many years, classical elasticity theory has been the main instrument for analyzing stress and deformation in these components. Nevertheless, a notable drawback of this classical approach is its failure to account for size

effects this refers to the phenomenon where the mechanical behavior of a structure is influenced by its absolute size, particularly when the characteristic dimensions approach the micro-scale [1]. This limitation is especially apparent in materials that possess an inherent internal microstructure, including polymers, composites, foams, bone, and granular materials. Traditional continuum mechanics, which presumes a point-like structure for material particles, fails to consider the effects of micro-rotations and the corresponding couple stresses that result from the interactions among these micro-constituents. To address this deficiency, generalized continuum theories have been formulated. Notably, micropolar elasticity (Cosserat theory) has surfaced as a robust and widely recognized framework [1 , 2]. This theory enhances the classical model by providing each material point with three additional rotational degrees of freedom (micro rotations), which are independent of the macroscopic displacement field. This addition results in asymmetric stress tensors and the formation of couple stress tensors, which are governed by a new set of constitutive parameters.

Importantly, these parameters include characteristic length scale parameters that fundamentally connect the macroscopic mechanical response to the underlying microstructure of the material [3]. The relationship between the structural response and these length scale parameters is fundamental to micropolar mechanics. These parameters serve as a physical representation of the scale at which micro-rotational effects gain significance in comparison to translational deformations. As the size of the structure diminishes or the features of the microstructure become more pronounced, the predictions made by micropolar theory significantly diverge from those of classical elasticity, thereby offering a more precise characterization of material behavior at reduced scales. Consequently, micropolar theory is essential for the analysis and design of micro-electro-mechanical systems (MEMS), advanced composites, and various metamaterials [3,4]. While micropolar theory has been applied to cylindrical structures in previous studies, most existing research has focused on specialized cases like functionally graded materials [5], thermoelastic behavior [6], or wave propagation [7]. However, a comprehensive numerical investigation specifically addressing the length-scale dependency in a uniform hollow cylinder under mechanical pressure using highly efficient methods remains limitedAlthough finite element methods (FEM) have been widely used, the application of the Generalized Differential Quadrature (GDQ) method for this particular boundary value problem is relatively unexplored, despite its recognized advantages in accuracy and computational efficiency for solving partial differential equations [8,9]. This paper therefore makes three key contributions to the field: First, it provides a systematic parametric analysis of the characteristic length scale parameter's influence on stress distributions in micropolar hollow cylinders. Second, it demonstrates the effective application of the GDQ method known for exceptional accuracy and computational efficiency to solve the intricate higher-order governing equations of micropolar elasticity in cylindrical coordinates. Third, it offers a critical comparison with classical elasticity solutions, distinctly outlining the conditions under which micropolar effects become significant. The novelty of this work lies in its focused investigation of length-scale effects in homogeneous micropolar cylinders using GDQ, filling an important gap between generalized continuum theories and efficient numerical computation for micro-scale applications. The main objectives are:

To establish the governing equations and boundary conditions for the axisymmetric scenario of a micropolar hollow cylinder under mechanical load.

To apply the robust GDQ numerical technique to discretize and resolve the resulting system of coupled ordinary differential equations. To perform a systematic parametric analysis, measuring the impact of the characteristic length scale parameter on the distribution of displacements, macro-stresses, and couple stresses. To offer a critical comparison with classical elasticity solutions, distinctly outlining the conditions under which micropolar effects are significant and must be considered. The utilization of micropolar theory in the context of cylindrical structures has garnered ongoing research interest. Pioneering studies and contemporary research have examined various dimensions of this topic. For example, Nejad et al. [5] conducted an analytical elastic analysis of functionally graded rotating thick-walled cylindrical shells, illustrating the significant influence of micropolar parameters. Ghorbani et al. [6] explored the thermoelastic behavior of a functionally graded micropolar cylindrical shell, emphasizing the interplay of thermo-microstructural effects. Additionally, Kumar and Sharma [7] investigated wave propagation in micropolar cylindrical porous media, uncovering complexities that classical models cannot address. Extensive reviews by prominent researchers, including Eremeyev et al. [1] and Lakes [2], reinforce the theoretical underpinnings and affirm the essential significance of this theory. In spite of these advancements, a thorough and concentrated numerical examination of the length scale dependency in a uniform hollow cylinder subjected to mechanical pressure, resolved through a highly efficient and accurate numerical approach, continues to be a significant research domain. Although numerous studies have utilized finite element methods (FEM), the use of the Generalized Differential Quadrature (GDQ) method for this particular boundary value problem

10.57647/jsm.2025.1704.13

is relatively limited. The GDQ method is well-known for its exceptional accuracy, computational efficiency, and straightforward implementation for solving partial differential equations, rendering it an ideal choice for addressing the intricate higher-order governing equations of micropolar elasticity [8,9].

Consequently, this article seeks to address this deficiency by offering a detailed numerical investigation into the length scale dependency of micropolar elasticity equations in a hollow cylinder subjected to internal and/or external pressure utilizing the GDQ method.

In most partial differential equations (PDE), due to the geometry, boundary conditions and complex loadings, it is not possible to solve them by analytical or semi-analytical method, so it is necessary to use numerical solution methods. Researchers use different methods to solve governing differential equations. Among these methods, finite element and finite difference methods can be mentioned, which are more popular for solving engineering problems and mathematical models. In the finite element method, the problem of a large system is divided into smaller and simpler parts called finite elements. Therefore, solving a complex system of partial differential equations leads to solving a system of ordinary differential equations or a system of algebraic equations. In the finite difference method, the derivative of functions is approximated by the differences of functions in different ways such as Taylor's method and with a certain error.

One of the main disadvantages of the above methods is that these methods require a lot of computing resources and time to divide the domain into a large number of elements and small nodes and solve a system of differential or algebraic equations for each node. This can lead to a huge amount of data and calculations, especially for 3D problems and fine meshes. Also, the results of these methods depend on the accuracy of the input data. Any error or uncertainty in the input data can negatively affect the reliability and validity of the results.

However, in many cases, problems require an accurate and fast solution for a limited number of network points. Research has shown that the generalized differential quadrature (GDQ) method is a simple, fast and accurate method for analyzing differential equations governing many problems. The Differential Quadrature method is recognized as one of the effective numerical methods for the solution of partial differential equations subject to boundary constraints. As it was originally presented by Bellman in 1972 [10], the derivative of a function at any given discrete point is approximated as a weighted linear combination of the values of the function at all discrete points in the computational domain. One of the main drawbacks to Bellman's original formulation was the difficult computation of weighting coefficients, which was overcome later by Kwan and Chang [11]. Shu and Richard [12] extended this formulation further and proposed the Generalized Differential Quadrature (GDQ) method that considerably enhanced the capability and robustness of the approach. The applicability of the Generalized Differential Quadrature method has been demonstrated in a wide range of solid mechanics problems. For example, Shishesaz et al. [13] used the GDQ approach for evaluating the radial and circumferential stress components in annular functionally graded plates of uniform thickness subjected to axisymmetric loading, taking into account the presence of a uniform radial magnetic field acting on the upper surface of the plate. Based on the same numerical framework, Panah et al. [14] examined the axisymmetric nonlinear bending response and thermal post-buckling behavior of functionally graded, saturated poroelastic circular plates under combined thermo-mechanical loading.

In this context, Rezaei et al. [15] addressed the nonlinear bending of functionally graded saturated porous microplates, whose governing equations and related boundary conditions were nondimensionalized, discretized through the use of the GDQ technique, and then solved by the iterative Newton–Raphson procedure. In addition, the elegance and effectiveness of the GDQ formulation have been demonstrated in its application to perform free vibration analyses on spherical shells and circular plates in a variety of studies [16–18].

More recently, Alinaghizadeh and Shariati [19] addressed the nonlinear bending of two-directional functionally graded circular and annular sector plates of variable thickness resting on nonlinear elastic foundations by combining the GDQ method with the Newton–Raphson iteration technique. On the other hand, Barati and Norouzi [20] examined the static torsional response of bidirectional functionally graded microtubes under a longitudinal magnetic field by considering a nonlocal elasticity model. Using the latter approach, some GDQ-based numerical solutions were compared to those obtained by using the Galerkin method with satisfactory agreement. Mohammadi et al. [21] conducted the free vibration analysis of double-walled functionally graded cylindrical microshells that are embedded in a viscoelastic foundation. In that study, the generalized differential quadrature method was used to discretize the governing equations of motion along with the related boundary conditions. In order to verify the accuracy of the developed numerical model, the obtained results were compared with those of the molecular dynamics simulation.

With regard to wave propagation problems, among others, Kaliraman and Poonia [22] considered elastic wave propagation at imperfect interfaces separating micropolar elastic solids and fluid-saturated porous solid half-spaces, while Kumar and Chawla [23] studied the effect of

rotational and stiffness parameters on surface wave propagation in an elastic layer lying on a generalized thermo-diffusive elastic half-space with imperfect boundary conditions. In another related contribution, Kumari [24] investigated reflection and transmission of longitudinal waves at the interface between a micropolar viscoelastic solid and a fluid-saturated incompressible porous medium.

Dehbani et al. [25 , 26] came up with very precise analytical solutions to investigate steady-state micropolar thermoelastic and magneto-thermoelastic responses in functionally graded materials. The material properties were supposed to be radially distributed in the form of a power-law distribution in their formulation. It was done using complex Fourier series along with power law functions to solve the governing heat conduction equations and also the Navier-type equations.

The main objectives of the present study are as follows:

(1) To derive the governing equations together with corresponding boundary conditions for an axisymmetric micropolar hollow cylinder under mechanical loading.

(2) To apply the generalized differential quadrature method as a powerful numerical tool to discretize and solve the system of resulting coupled ODEs efficiently.

(3) Perform a systematic parametric study in order to ascertain the effects of the characteristic length scale parameter on the displacement fields, macro-stress components, and couple stresses.

(4) The detailed comparison with classical elasticity solutions for the purpose of determining the conditions when the micropolar effects become important and cannot be neglected. The paper is organized as follows:

The governing equations are derived within the framework of micropolar elasticity in Section 2. The generalized differential quadrature method, used to discretize the governing equations and the related boundary conditions for the computation of the weighting coefficients, is introduced in Section 3. In Section 4 the numerical results are presented and graphically shown, whereas the proposed solution procedure is tested against the classical elasticity model and micropolar elasticity model considering different values of the length scale parameter and boundary conditions. Concluding remarks are summarized in Section 5.

2. Governing equations

2.1. Fundamental concepts and assumptions

Micropolar elasticity theory extends classical continuum mechanics by introducing additional rotational degrees of freedom (micro-rotations) at each material point. The fundamental assumptions that each material point possesses three translational (u_i) and three rotational (Φ_i) degrees of freedom. The stress tensor becomes asymmetric ($\sigma_{ij} \neq \sigma_{ji}$) and Couple stresses ($m_{ij}$) appear as work-conjugate to micro-rotation gradients. Also, The theory introduces three characteristic length parameters (l_1,l_2) linking macroscopic response to microstructure.

2.2. Step-by-step derivation

The derivation begins with the conservation laws for linear and angular momentum in polar coordinates:

-Linear Momentum Balance:

$$\frac{\partial \sigma_{rr}}{\partial r} + \frac{1}{r}\frac{\partial \sigma_{r\theta}}{\partial \theta} + \frac{\sigma_{rr} - \sigma_{\theta\theta}}{r} = 0$$

-Angular Momentum Balance

$$\frac{\partial m_{rz}}{\partial r} + \frac{1}{r}\frac{\partial m_{\theta z}}{\partial \theta} + \frac{m_{rz}}{r} + \sigma_{r\theta} - \sigma_{\theta r} = 0$$

-The constitutive relations for linear isotropic micropolar materials are

$$\sigma_{ij} = \lambda \varepsilon_{kk}\delta_{ij} + (2\mu + \kappa)\varepsilon_{ij} + \kappa \varepsilon_{ji} = 0$$

$$m_{ij} = \alpha \varphi_{k,k}\delta_{ij} + \beta \varphi_{i,j} + \gamma \varphi_{i,j} = 0$$

-Through mathematical transformations using stress functions and, we obtain the final governing equations in polar coordinates:

$$\frac{\partial}{\partial r}(\psi - l_i^2 \nabla^2 \psi) = -2(1-\nu) l_2^2 \frac{1}{r}\frac{\partial}{\partial \theta}(\nabla^2 \Phi)$$

$$\frac{1}{r}\frac{\partial}{\partial \theta}(\psi - l_i^2 \nabla^2 \psi) = 2(1-\nu) l_2^2 \frac{\partial}{\partial r}(\nabla^2 \Phi)$$

2.3. Comparison with classical elasticity

The principal distinctions between micropolar elasticity and classical elasticity theories are outlined in Table 1.

Table 1. Comparison between Classical and Micropolar Elasticity

Feature	Classical Elasticity	Micropolar Elasticity
DOF per point	3 translations	3 translations + 3 rotations
Stress tensor	Symmetric ($\sigma_{ij} = \sigma_{ji}$)	Asymmetric ($\sigma_{ij} \neq \sigma_{ji}$)
Additional stresses	None	Couple stresses (m_ij)
Size effects	captured	Captured via length parameters
Governing equations	Navier's equations	Extended Navier equations + microrotation balance

10.57647/jsm.2025.1704.13

2.4. Physical interpretation of micropolar parameters

-The characteristic length parameters have clear physical meanings:

- $l_1 = l_c$ (torsional characteristic length): Represents the scale at which micro-rotational effects become significant in torsion
- $l_2 = l_b$ (bending characteristic length): Characterizes the influence of microstructure in bending-dominated deformations

These parameters fundamentally connect the macroscopic mechanical response to the underlying material microstructure, making micropolar theory essential for micro-scale applications. Figure 1 schematically depicts a hollow micro-cylinder with inner and outer radii denoted by a and b, respectively.

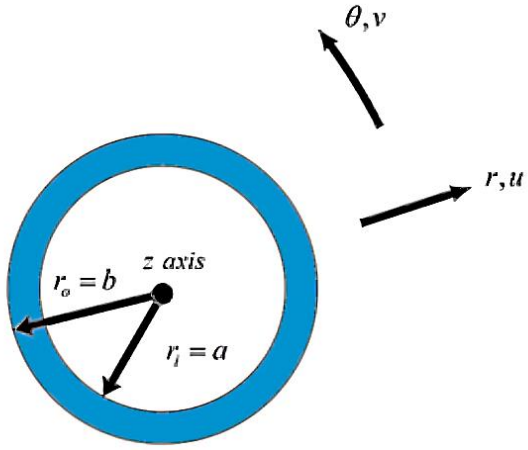

Figure 1. shematic geometry of the Isotropic hollow microcylinder

Two-dimensional micropolar plane strain equations of elasticity considering size effects for a linear elastic isotropic hollow cylinder in polar coordinates shown in Figure 1 are as follows [27]:

$$\frac{\partial}{\partial r}(\psi - l_1^2\nabla^2\psi) = -2(1-\nu)l_2^2\frac{1}{r}\frac{\partial}{\partial\theta}(\nabla^2\Phi) \qquad (1\text{-a})$$

$$\frac{1}{r}\frac{\partial}{\partial\theta}(\psi - l_1^2\nabla^2\psi) = 2(1-\nu)l_2^2\frac{\partial}{\partial r}(\nabla^2\Phi) \qquad (1\text{-b})$$

Where l_c, l_b, ν and ∇^2respectively, torsional characteristic length, bending characteristic length, Poisson's ratio and Laplacian operator are in cylindrical coordinates and are defined as follows:

$$\nu = \frac{\lambda}{(\kappa + 2\lambda + 2\mu)} \qquad (2)$$

$$l_c^2 = \frac{\gamma(\kappa+\mu)}{\kappa(\kappa+2\mu)} \qquad (3)$$

$$l_b^2 = \frac{\gamma}{2(\kappa+2\mu)} \qquad (4)$$

$$\nabla^2 = \frac{\partial^2}{\partial r^2} + \frac{1}{r}\frac{\partial}{\partial r} + \frac{1}{r^2}\frac{\partial^2}{\partial\theta^2} \qquad (5)$$

In the framework of micropolar elasticity, the force stress and couple stress tensors are expressed in terms of the stress functions Φ and Ψ as follows:

$$\sigma_{rr} = \frac{1}{r}\frac{\partial\phi}{\partial r} + \frac{1}{r^2}\frac{\partial^2\phi}{\partial\theta^2} - \frac{1}{r}\frac{\partial^2\psi}{\partial r\partial\theta} + \frac{1}{r^2}\frac{\partial\psi}{\partial\theta}$$

$$\sigma_{\theta\theta} = \frac{\partial^2\phi}{\partial r^2} + \frac{1}{r}\frac{\partial^2\psi}{\partial r\partial\theta} - \frac{1}{r^2}\frac{\partial\psi}{\partial\theta}$$

$$\tau_{r\theta} = -\frac{1}{r}\frac{\partial^2\phi}{\partial r\partial\theta} + \frac{1}{r^2}\frac{\partial\phi}{\partial\theta} - \frac{1}{r}\frac{\partial\psi}{\partial r} - \frac{1}{r^2}\frac{\partial^2\psi}{\partial\theta^2} \qquad (6)$$

$$\tau_{\theta\ r} = -\frac{1}{r}\frac{\partial^2\phi}{\partial r\partial\theta} + \frac{1}{r^2}\frac{\partial\phi}{\partial\theta} + \frac{\partial^2\psi}{\partial r^2}$$

$$m_{\theta\ z} = \frac{1}{r}\frac{\partial\psi}{\partial\theta}$$

$$m_{rz} = \frac{\partial\psi}{\partial r}$$

Upon solving the governing Eq. 1 using the GDQ method, the force stress and couple stress components are subsequently obtained from the relations given in Eq. (6). By substituting Eqs. (6) in micropolar elasticity Eq. (1), yields

$$-\frac{\mu}{\kappa}\frac{1}{r^2}\frac{\partial\psi}{\partial r} - \frac{1}{r}\frac{1}{r}\frac{\partial\psi}{\partial r} + \frac{\mu}{\kappa}\frac{1}{r}\frac{\partial^2\psi}{\partial r^2} - \frac{\mu}{\kappa}\frac{2}{r^3}\frac{\partial^2\psi}{\partial\theta^2}$$

$$-\frac{(\kappa+\lambda+2\mu)}{(\kappa+2\lambda+2\mu)}\frac{1}{r}\frac{1}{r^2}\frac{\partial^2\psi}{\partial\theta^2}$$

$$-\frac{\lambda}{(\kappa+2\lambda+2\mu)}\frac{1}{r}\frac{1}{r^2}\frac{\partial^2\psi}{\partial\theta^2} - \frac{1}{r}\frac{1}{r^2}\frac{\partial^2\psi}{\partial\theta^2} + \frac{1}{r}\frac{\partial^2\psi}{\partial r^2}$$

$$+\frac{\mu}{\kappa}\frac{1}{r^2}\frac{\partial^3\psi}{\partial\theta^2\partial r} + \frac{(\kappa+\mu)}{\kappa}\frac{\partial^3\psi}{\partial r^3} \qquad (7\text{-a})$$

$$+\frac{(\kappa+\lambda+2\mu)}{(\kappa+2\lambda+2\mu)}\frac{1}{r}\frac{1}{r}\frac{\partial^3\psi}{\partial r\partial^2\theta}$$

$$+\frac{\lambda}{(\kappa+2\lambda+2\mu)}\frac{1}{r}\frac{1}{r}\frac{\partial^3\psi}{\partial r\partial^2\theta}$$

$$-(\kappa+2\mu)\frac{1}{\gamma}\frac{\partial\psi}{\partial r} - \frac{(\kappa+2\mu)\gamma_t}{(\kappa+2\lambda+2\mu)}\frac{1}{r}T_{,\theta} = 0$$

10.57647/jsm.2025.1704.13

$$-\frac{\kappa+\lambda+2\mu}{(\kappa+2\lambda+2\mu)}\frac{1}{r^2}\frac{\partial\Phi}{\partial r}+\frac{\kappa+\lambda+2\mu}{(\kappa+2\lambda+2\mu)}\frac{1}{r}\frac{\partial^2\Phi}{\partial r^2}$$

$$-2\frac{\kappa+\lambda+2\mu}{(\kappa+2\lambda+2\mu)}\frac{1}{r^3}\frac{\partial^2\Phi}{\partial\theta^2}$$

$$+\frac{(\kappa+\lambda+2\mu)}{(\kappa+2\lambda+2\mu)}\frac{\partial^3\Phi}{\partial r^3}+\frac{\kappa+\lambda+2\mu}{(\kappa+2\lambda+2\mu)}\frac{1}{r^2}\frac{\partial^3\Phi}{\partial\theta^2\partial r}$$

$$-\frac{\lambda}{(\kappa+2\lambda+2\mu)}\frac{1}{r^2}\frac{\partial^2\psi}{\partial r\partial\theta}$$

$$+\frac{\lambda}{(\kappa+2\lambda+2\mu)}\frac{1}{r}\frac{\partial^3\psi}{\partial r^2\partial\theta}+\frac{\lambda}{(\kappa+2\lambda+2\mu)}\frac{2}{r^3}\frac{\partial\psi}{\partial\theta}$$

$$-\frac{\lambda}{(\kappa+2\lambda+2\mu)}\frac{1}{r^2}\frac{\partial^2\psi}{\partial\theta\partial r}$$

$$-\frac{(\kappa+\lambda+2\mu)}{(\kappa+2\lambda+2\mu)}\frac{1}{r^2}\frac{\partial^2\psi}{\partial r\partial\theta}$$

$$+\frac{(\kappa+\lambda+2\mu)}{(\kappa+2\lambda+2\mu)}\frac{1}{r}\frac{\partial^3\psi}{\partial r^2\partial\theta}$$

$$+\frac{(\kappa+\lambda+2\mu)}{(\kappa+2\lambda+2\mu)}\frac{2}{r^3}\frac{\partial\psi}{\partial\theta}$$

$$-\frac{(\kappa+\lambda+2\mu)}{(\kappa+2\lambda+2\mu)}\frac{1}{r^2}\frac{\partial^2\psi}{\partial\theta\partial r}+\frac{(\kappa+\mu)}{\kappa}\frac{1}{r}\frac{1}{r}\frac{\partial^2\psi}{\partial r\partial\theta}$$

$$+\frac{(\kappa+\mu)}{\kappa}\frac{1}{r}\frac{1}{r^2}\frac{\partial^3\psi}{\partial\theta^3}$$

$$+\frac{\mu}{\kappa}\frac{1}{r}\frac{\partial^3\psi}{\partial r^2\partial\theta}+\frac{1}{r}\frac{1}{r}\frac{\partial^2\psi}{\partial r\partial\theta}-\frac{1}{r}\frac{1}{r^2}\frac{\partial\psi}{\partial\theta}$$

$$+\frac{1}{r}\frac{1}{r}\frac{\partial^2\psi}{\partial r\partial\theta}-\frac{1}{r}\frac{1}{r^2}\frac{\partial\psi}{\partial\theta}$$

$$-\frac{1}{\gamma}(\kappa+2\mu)\frac{1}{r}\frac{\partial\psi}{\partial\theta}+\frac{(\kappa+2\mu)\gamma_t}{(\kappa+2\lambda+2\mu)}T_{,r}=0 \qquad (7\text{-b})$$

3. Numerical analysis

3.1. Advantages of the GDQ method

In this work, the GDQ method is adopted because it has well-recognized advantages compared with other conventional numerical approaches, such as FEM and FDM. In detail, GDQ is capable of obtaining high levels of numerical accuracy and rapid convergence by using a relatively limited number of grid points. This is due to the fact that in GDQ derivatives at a given node can be directly represented as a weighted linear combination of the function values at all discretized points in the computational domain. The consequence of such feature is that the adoption of dense meshing is totally unnecessary; this is the major bottleneck of the FEM when higher-order differential operators should be considered. Secondly, the method is straightforward to implement for complex geometries and high-order differential equations, such as the governing equations of micropolar elasticity, which are fourth-order in this formulation. While FDM is simpler, it often requires a dense grid for comparable accuracy, increasing computational cost. The application of GDQ to the current boundary value problem demonstrates its exceptional capability to handle the intricate coupling and size-dependent terms of micropolar theory efficiently.

3.2. Discretization

3.2.1. *Domain*

To discretize the governing equations given in Eq. (1), the generalized differential quadrature (GDQ) method is adopted. In most previous studies, both uniform and non-uniform grid distributions have commonly been employed; the latter is often based on the Chebyshev–Gauss–Lobatto scheme, described below [14]:

$$x_n = x_1 + \frac{0.5(1-x_1)(n-1)}{(N-1)} \qquad 1 \le n \le N$$

$$x_n = x_1 + 0.5(1-x_1) \qquad (8)$$

$$\left\{1-cos\left[\frac{(n-1)\pi}{(N-1)}\right]\right\} \qquad 1 \le n \le N$$

In this article, uniform distribution (7) is used to increase the speed of convergence and the accuracy of the solution. Using the differential quadratic method, there is no limit in applying boundary conditions, and all types of boundary conditions can be applied at each edge of the sector. The uniform grid point distribution in a two-dimensional domain and in polar coordinates is shown in Figure 2.

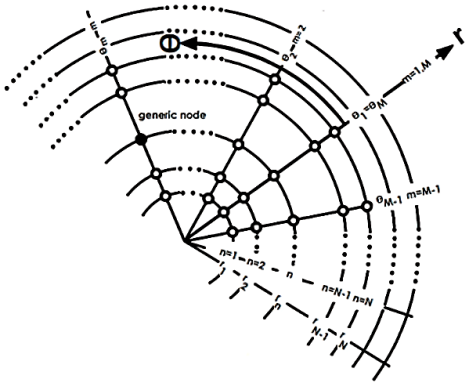

Figure2. discretized polar grid

10.57647/jsm.2025.1704.13

Figure 2 shows the discretized computational domain composed of M radial grid lines and N circumferential grid lines.

Accordingly, the coordinates of the grid point at the $(m,)$-th position in the discrete domain are given by the following relation [15]:

$$\begin{aligned} g &= g(m,n) && 1 \le n \le N \\ &= (m-1)N + n && 1 \le m \le M \end{aligned} \tag{9}$$

3.3. Numerical derivatives

The weight coefficient of the generalized differential quadratic method, $L_n(x)$, is classically defined as the nth derivative of the Lagrange interpolation polynomial in $x = x_n$.

By using the discrete values of the function, denoted by, $\{y_n | 1 \le n \le N\}$, it is possible to approximate the continuous variation of the function along the x-direction by a set of Lagrange interpolation polynomials, $\{L_n(x) | 1 \le n \le N\}$, so that the first derivative of the function in $x = x_n$, for example, $\{L_n^{'}(x) | 1 \le n \le N\}$ through the set of GDQ coefficients and it is defined as follows:

$$y(x) = \sum_{n=1}^{N} y_n L_n(x)$$

$$L_n(x) \equiv \frac{\prod_{\substack{m=1 \\ m\neq n}}^{N}(x - x_m)}{(x - x_n)\prod_{\substack{m=1 \\ m\neq n}}^{N}(x_n - x_m)}$$

$$y'(x) = \sum_{n=}^{N} y_n\, L_n'(x)$$

$$L_n'(x) \equiv \frac{1}{\prod_{\substack{m=1 \\ m\neq n}}^{N}(x_n - x_m)} \sum_{k=1}^{N} \prod_{\substack{m=1 \\ m\neq n \\ m\neq k}}^{N} (x - x_m) \tag{10}$$

$$L_n'(x_n) \equiv -\sum_{\substack{m=1 \\ m\neq n}}^{N} L_n'(x_n) \qquad n = s$$

$$L_n'(x_s) \equiv \frac{\prod_{\substack{m=1 \\ m\neq s}}^{N}(x_s - x_m)}{(x_s - x_n)\prod_{\substack{m=1 \\ m\neq n}}^{N}(x_n - x_m)} \qquad n \neq s$$

The vectors related to numerical derivative coefficients A_i, B_i, C_i and D_i respectively from the 0th to the 4th order are displayed as follows:

$$\begin{aligned} A_i &= \begin{bmatrix} a_i^1 & a_i^1 & ,,, & a_i^k & a_i^{N-1} & a_i^N \end{bmatrix}^T \\ B_i &= \begin{bmatrix} b_i^1 & b_i^1 & ,,, & b_i^k & b_i^{N-1} & b_i^N \end{bmatrix}^T \\ C_i &= \begin{bmatrix} c_i^1 & c_i^1 & ,,, & c_i^k & c_i^{N-1} & c_i^N \end{bmatrix}^T \\ D_i &= \begin{bmatrix} d_i^1 & d_i^1 & ,,, & d_i^k & d_i^{N-1} & d_i^N \end{bmatrix}^T \end{aligned} \tag{11}$$

For instance, can be stated in terms of the GDQ coefficients as In Eqs. (11), the coefficients related to the first- through fourth-order derivatives, a_i^k, b_i^k, c_i^k and d_i^k, are introduced based on the generalized differential quadrature formulation as presented hereafter [14]:

$$a_i^k \equiv \frac{\prod_{\substack{m=1 \\ m\neq i}}^{N}(x_i - x_m)}{(x_i - x_k)\prod_{\substack{m=1 \\ m\neq k}}^{N}(x_k - x_m)}$$

$$a_i^k \equiv -\sum_{\substack{m=1 \\ m\neq i}}^{N} a_i^m$$

$$b_i^k \equiv \frac{\prod_{\substack{m=1 \\ m\neq i}}^{N}(x_i - x_m)}{(x_i - x_k)\prod_{\substack{m=1 \\ m\neq k}}^{N}(x_k - x_m)}$$

$$b_i^k \equiv -\sum_{\substack{m=1 \\ m\neq i}}^{N} b_i^m \tag{12}$$

$$c_i^k \equiv \frac{\prod_{\substack{m=1 \\ m\neq i}}^{N}(x_i - x_m)}{(x_i - x_k)\prod_{\substack{m=1 \\ m\neq k}}^{N}(x_k - x_m)}$$

$$c_i^k \equiv -\sum_{\substack{m=1 \\ m\neq i}}^{N} c_i^m$$

$$d_i^k \equiv \frac{\prod_{\substack{m=1 \\ m\neq i}}^{N}(x_i - x_m)}{(x_i - x_k)\prod_{\substack{m=1 \\ m\neq k}}^{N}(x_k - x_m)}$$

$$d_i^k \equiv -\sum_{\substack{m=1 \\ m\neq i}}^{N} d_i^m$$

The partial derivatives on the whole field ($LS\sigma_m^n$) with respect to r and are defined as follows [15]:

$$\left[\frac{\partial(LS\sigma_m^n)}{\partial r} \quad \frac{\partial^2(LS\sigma_m^n)}{\partial r^2} \quad \frac{\partial^3(LS\sigma_m^n)}{\partial r^3} \quad \frac{\partial^4(LS\sigma_m^n)}{\partial r^4}\right]$$

$$= [A^n \quad B^n \quad C^n \quad D^n] H_N^{m.M} H_{MN}^{\sigma.\Sigma} LS$$

$$\left[\frac{\partial(LS\sigma_m^n)}{\partial\theta} \quad \frac{\partial^2(LS\sigma_m^n)}{\partial\theta^2} \quad \frac{\partial^3(LS\sigma_m^n)}{\partial\theta^3} \quad \frac{\partial^4(LS\sigma_m^n)}{\partial\theta^4}\right]$$

$$= [A^m \quad B^m \quad C^m \quad D^m] R^n H_{MN}^{\sigma.\Sigma} LS$$

$$\left[\frac{\partial^2(LS\sigma_m^n)}{\partial r\partial\theta} \quad \frac{\partial^3(LS\sigma_m^n)}{\partial r^2\partial\theta} \quad \frac{\partial^3(LS\sigma_m^n)}{\partial r\partial\theta^2} \quad \frac{\partial^4(LS\sigma_m^n)}{\partial r^2\partial\theta^2}\right.$$

$$\left.\frac{\partial^4(LS\sigma_m^n)}{\partial r^3\partial\theta} \quad \frac{\partial^4(Ls\sigma_m^n)}{\partial r\partial\theta^3}\right] \tag{13}$$

$$[A^n A r^m \quad B^n A r^m \quad A^n B r^m \quad B^n B r^m \quad C^n A r^m \quad A^n C r^m]$$

$$H_{MN}^{\sigma.\Sigma} LS$$

3.4. Discrete field equations

By substituting Eqs. (2) - (5) in micropolar elasticity Eq.(7-a) and Eq.(7-b) and their expansion, yields:

$$\frac{1}{r^2}\frac{\partial^3\psi}{\partial\theta^2\partial r} + \frac{\partial^3\psi}{\partial r^3} + \frac{1}{r}\frac{\partial^2\psi}{\partial r^2} - \frac{2}{r^3}\frac{\partial^2\psi}{\partial\theta^2}$$

$$+\left[-\frac{1}{l_1^2} - \frac{1}{r^2}\right]\frac{\partial\psi}{\partial r} - 2(1-\nu)\left(\frac{l_2^2}{l_1^2}\right)\frac{1}{r}\frac{\partial^3\Phi}{\partial r^2\partial\theta}$$

$$-2(1-\nu)\left(\frac{l_2^2}{l_1^2}\right)\frac{1}{r^3}\frac{\partial^3\Phi}{\partial\theta^3} \tag{14-a}$$

$$-2(1-\nu)\left(\frac{l_2^2}{l_1^2}\right)\frac{1}{r^2}\frac{\partial^2\Phi}{\partial r\partial\theta} = 0$$

$$-l_1^2\frac{1}{r}\frac{\partial^3\psi}{\partial r^2\partial\theta} - l_1^2\frac{1}{r^3}\frac{\partial^3\psi}{\partial\theta^3} - l_1^2\frac{1}{r^2}\frac{\partial^2\psi}{\partial r\partial\theta}$$

$$+\frac{1}{r}\frac{\partial\psi}{\partial\theta} - 2(1-\nu)l_2^2\frac{\partial^3\Phi}{\partial r^3}$$

$$-2(1-\nu)l_2^2\frac{1}{r^2}\frac{\partial^3\Phi}{\partial\theta^2\partial r} - 2(1-\nu)l_2^2\frac{1}{r}\frac{\partial^2\Phi}{\partial r^2} \tag{14-b}$$

$$+4(1-\nu)l_2^2\frac{1}{r^3}\frac{\partial^2\Phi}{\partial\theta^2} + 2(1-\nu)l_2^2\frac{1}{r^2}\frac{\partial\Phi}{\partial r} = 0$$

By dividing the sides of relation (14-a) by $-l_1^2$ and the sides of relation (14-b) by $-2(1-\nu)l_2^2$ give

$$-l_1^2\left(\frac{1}{-l_1^2}\right)\frac{1}{r^2}\frac{\partial^3\psi}{\partial\theta^2\partial r} - l_1^2\left(\frac{1}{-l_1^2}\right)\frac{\partial^3\psi}{\partial r^3}$$

$$-l_1^2\left(\frac{1}{-l_1^2}\right)\frac{1}{r}\frac{\partial^2\psi}{\partial r^2} + 2l_1^2\left(\frac{1}{-l_1^2}\right)\frac{1}{r^3}\frac{\partial^2\psi}{\partial\theta^2}$$

$$+\left[1 + l_1^2\frac{1}{r^2}\right]\left(\frac{1}{-l_1^2}\right)\frac{\partial\psi}{\partial r}$$

$$+2(1-\nu)l_2^2\left(\frac{1}{-l_1^2}\right)\frac{1}{r}\frac{\partial^3\Phi}{\partial r^2\partial\theta} \tag{15-a}$$

$$+2(1-\nu)l_2^2\left(\frac{1}{-l_1^2}\right)\frac{1}{r^3}\frac{\partial^3\Phi}{\partial\theta^3}$$

$$+2(1-\nu)l_2^2\left(\frac{1}{-l_1^2}\right)\frac{1}{r^2}\frac{\partial^2\Phi}{\partial r\partial\theta} = 0$$

$$-l_1^2\left(\frac{1}{-2(1-\nu)l_2^2}\right)\frac{1}{r}\frac{\partial^3\psi}{\partial r^2\partial\theta}$$

$$-l_1^2\left(\frac{1}{-2(1-\nu)l_2^2}\right)\frac{1}{r^3}\frac{\partial^3\psi}{\partial\theta^3}$$

$$-l_1^2\left(\frac{1}{-2(1-\nu)l_2^2}\right)\frac{1}{r^2}\frac{\partial^2\psi}{\partial r\partial\theta}$$

$$+\left(\frac{1}{-2(1-\nu)l_2^2}\right)\frac{1}{r}\frac{\partial\psi}{\partial\theta}$$

$$-2(1-\nu)l_2^2\left(\frac{1}{-2(1-\nu)l_2^2}\right)\frac{\partial^3\Phi}{\partial r^3} \tag{15-b}$$

$$-2(1-\nu)l_2^2\left(\frac{1}{-2(1-\nu)l_2^2}\right)\frac{1}{r^2}\frac{\partial^3\Phi}{\partial\theta^2\partial r}$$

$$-2(1-\nu)l_2^2\left(\frac{1}{-2(1-\nu)l_2^2}\right)\frac{1}{r}\frac{\partial^2\Phi}{\partial r^2}$$

$$+4(1-\nu)l_2^2\left(\frac{1}{-2(1-\nu)l_2^2}\right)\frac{1}{r^3}\frac{\partial^2\Phi}{\partial\theta^2}$$

$$+2(1-\nu)l_2^2\left(\frac{1}{-2(1-\nu)l_2^2}\right)\frac{1}{r^2}\frac{\partial\Phi}{\partial r} = 0$$

By simplifying relations are obtained as

$$\frac{1}{r^2}\frac{\partial^3\psi}{\partial\theta^2\partial r} + \frac{\partial^3\psi}{\partial r^3} + \frac{1}{r}\frac{\partial^2\psi}{\partial r^2} - \frac{2}{r^3}\frac{\partial^2\psi}{\partial\theta^2}$$

$$+\left[\frac{1}{-l_1^2} - \frac{1}{r^2}\right]\frac{\partial\psi}{\partial r} - 2(1-\nu)\left(\frac{l_2^2}{l_1^2}\right)\frac{1}{r}\frac{\partial^3\Phi}{\partial r^2\partial\theta} \tag{16-a}$$

$$-2(1-\nu)\left(\frac{l_2^2}{l_1^2}\right)\frac{1}{r^3}\frac{\partial^3\Phi}{\partial\theta^3}$$

$$-2(1-\nu)\left(\frac{l_2^2}{l_1^2}\right)\frac{1}{r^2}\frac{\partial^2\Phi}{\partial r\partial\theta} = 0$$

10.57647/jsm.2025.1704.13

$$\left(\frac{l_1^2}{2(1-\nu)l_2^2}\right)\frac{1}{r}\frac{\partial^3\psi}{\partial r^2\partial\theta}+\left(\frac{l_1^2}{2(1-\nu)l_2^2}\right)\frac{1}{r^3}\frac{\partial^3\psi}{\partial\theta^3}$$
$$+\left(\frac{l_1^2}{2(1-\nu)l_2^2}\right)\frac{1}{r^2}\frac{\partial^2\psi}{\partial r\partial\theta}-\left(\frac{1}{2(1-\nu)l_2^2}\right)\frac{1}{r}\frac{\partial\psi}{\partial\theta}$$
$$+\frac{\partial^3\Phi}{\partial r^3}+\frac{1}{r^2}\frac{\partial^3\Phi}{\partial\theta^2\partial r}+\frac{1}{r}\frac{\partial^2\Phi}{\partial r^2} \quad (16\text{-b})$$
$$-2\frac{1}{r^3}\frac{\partial^2\Phi}{\partial\theta^2}-\frac{1}{r^2}\frac{\partial\Phi}{\partial r}=0$$

To simplify Eqs. (16), we define the coefficients as follows:

$$P_1(r)=\frac{1}{r^2} \qquad P_2(r)=\frac{1}{r} \qquad P_3(r)=-\frac{2}{r^3}$$
$$P_4(r)=-K_1-\frac{1}{r^2} \qquad P_5(r)=-K_3\frac{1}{r}$$
$$P_6(r)-K_3\frac{1}{r^3} \qquad P_7(r)=-K_3\frac{1}{r^2} \qquad P_8(r)=\frac{1}{K_3}\frac{1}{r} \quad (17)$$
$$P_9(r)=\frac{1}{K_3}\frac{1}{r^3} \qquad P_{10}(r)=\frac{1}{K_3}\frac{1}{r^2} \qquad P_{11}(r)=\frac{-1}{2K_2}\frac{1}{r}$$
$$P_{12}(r)=\frac{1}{r^2} \qquad P_{13}(r)=\frac{1}{r} \qquad P_{14}(r)=\frac{-2}{r^3}$$
$$P_{15}(r)=\frac{-1}{r^2}$$

which K_2, K_1 and $K_3$are expressed as:

$$K_1=\frac{1}{l_t^2} \qquad K_2=(1-\nu)l_b^2 \qquad K_3=2K_1K_2 \quad (18)$$

By substituting Eq. (16) in Eqs. (15), yields:

$$P_1(r)\frac{\partial^3\psi}{\partial\theta^2\partial r}+\frac{\partial^3\psi}{\partial r^3}+P_2(r)\frac{\partial^2\psi}{\partial r^2}$$
$$+P_3(r)\frac{\partial^2\psi}{\partial\theta^2}+P_4(r)\frac{\partial\psi}{\partial r} \quad (19\text{-a})$$
$$+P_5(r)\frac{\partial^3\Phi}{\partial r^2\partial\theta}+P_6(r)\frac{\partial^3\Phi}{\partial\theta^3}+P_7(r)\frac{\partial^2\Phi}{\partial r\partial\theta}=0$$

$$P_8(r)\frac{\partial^3\psi}{\partial r^2\partial\theta}+P_9(r)\frac{\partial^3\psi}{\partial\theta^3}+P_{10}(r)\frac{\partial^2\psi}{\partial r\partial\theta}$$
$$+P_{11}(r)\frac{\partial\psi}{\partial\theta}+\frac{\partial^3\Phi}{\partial r^3}+P_{12}(r)\frac{\partial^3\Phi}{\partial\theta^2\partial r} \quad (19\text{-b})$$
$$+P_{13}(r)\frac{\partial^2\Phi}{\partial r^2}+P_{14}(r)\frac{\partial^2\Phi}{\partial\theta^2}+P_{15}(r)\frac{\partial\Phi}{\partial r}=0$$

By substituting Eqs. (13) ref. [15] in Eqs. (19), yields:

$$P_1(r)A_n\mathrm{Br}_m s+C_nH(\mathrm{m,M,N})s$$
$$+P_2(r)B_nH(\mathrm{m,M,N})s+P_3(r)B_mR_ns \quad (20\text{-a})$$
$$+P_4(r)A_nH(\mathrm{m,M,N})s+P_5(r)B_n\mathrm{Ar}_m f$$
$$+P_6(r)C_mR_nf+P_7(r)A_n\mathrm{Ar}_m f=0$$

$$P_8(r)B_n\mathrm{Ar}_m s+P_9(r)C_mR_ns+P_{10}(r)A_n\mathrm{Ar}_m s$$
$$+P_{11}(r)A_mR_ns+C_nH(\mathrm{m,M,N})f \quad (20\text{-b})$$
$$+P_{12}(r)A_n\mathrm{Br}_m f+P_{13}(r)B_nH(\mathrm{m,M,N})f$$
$$+P_{14}(r)B_mR_nf+P_{15}(r)A_nH(\mathrm{m,M,N})f=0$$

3.5. Discrete boundary conditions

The differential equations of field variables Φ and $\psi$are of order 2 related to r and θ, so we need 8 boundary conditions to solve Eqs. (20).

Four boundary conditions for a microcylinder under internal and external pressure are defined as follows [28]:

$$\sigma_{rr}-l^2\left[\begin{matrix}\frac{d^2\sigma_{rr}}{dr^2}+\frac{1}{r}\left(\frac{d\sigma_{rr}}{dr}-\frac{d\sigma_{\theta\theta}}{dr}\right)\\-\frac{2}{r^2}(\sigma_{rr}-\sigma_{\theta\theta})\end{matrix}\right]_{r=r_i}=-P_i$$
$$l^2\left.\frac{d\sigma_{rr}}{dr}\right|_{r=r_i}=0 \quad (21)$$
$$\sigma_{rr}-l^2\left[\begin{matrix}\frac{d^2\sigma_{rr}}{dr^2}+\frac{1}{r}\left(\frac{d\sigma_{rr}}{dr}-\frac{d\sigma_{\theta\theta}}{dr}\right)\\-\frac{2}{r^2}(\sigma_{rr}-\sigma_{\theta\theta})\end{matrix}\right]_{r=r_o}=-P_o$$
$$l^2\left.\frac{d\sigma_{rr}}{dr}\right|_{r=r_o}=0$$

Also, 4 continuity conditions are equal to:

$$\left.\frac{\partial\Phi}{\partial\theta}\right|_{m=1}^{n}=\left.\frac{\partial\Phi}{\partial\theta}\right|_{m=M}^{n} \qquad \Phi|_{m=1}^{n}=\Phi|_{m=M}^{n}$$
$$\left.\frac{\partial\psi}{\partial\theta}\right|_{m=1}^{n}=\left.\frac{\partial\psi}{\partial\theta}\right|_{m=M}^{n} \qquad \psi|_{m=1}^{n}=\psi_{m=M}^{n} \quad (22)$$

In order to discretize the boundary conditions, we place Eq. (13) in Eq. (21), we have

$$\sigma_{rr}=P(2)A_nH(m,M,N)f+P(1)B_mR_nf$$

$$-P(2)A_nAr_ms + P(1)A_mR_ns$$

$$\sigma_{\theta\theta} = B_nH(m,M,N)f$$

$$+P(2)A_nAr_ms - p(1)A_mR_ns$$

$$\frac{d\sigma_{rr}}{dr} = -P(1)A_nH(m,M,N)f$$

$$+P(2)B_nH(m,M,N)f + P(3)B_mR_nf$$

$$+P(1)A_nBr_mf + 2P(1)A_nAr_ms$$

$$-P(2)B_nAr_ms + P(3)A_mR_ns$$

$$\frac{d^2\sigma_{rr}}{dr^2} = -P(3)A_nH(m,M,N)f \qquad (23)$$

$$-2P(1)B_nH(m,M,N)f + P(2)C_nH(m,M,N)f$$

$$+6P(1)^2B_mR_nf + 2P(3)A_nBr_mf + P(1)B_nBr_mf$$

$$+3P(3)A_nAr_ms + 3P(1)B_nAr_ms$$

$$-P(2)C_nAr_ms + 6P(1)^2A_mR_ns$$

$$\frac{d\sigma_{\theta\theta}}{dr} = C_nH(m,M,N)f - 2P(1)A_nAr_ms$$

$$+P(2)B_nAr_ms - P(3)A_mR_ns$$

The use of the GDQ method in static problems results in a system of algebraic equations, which can be obtained by solving this system of its unknowns, which are the values of the function at nodal points.

4. Numerical results and discussion

In the previous sections, governing relations, discretization of governing equations, discrete boundary conditions and assembling using GDQ method for the problem of micropolar elasticity of cylinder in static state were presented.

The assumptions of this section are presented in Table 2.

Table 2. Parameter values in the Example of micro-cylinder

Parameter	Value	Unit
r_i	1	μm
r_o	5	μm
P_i	10	MPa
$P_\circ$	0	MPa
ν	0.3	--
n, m (Number of Node)	16	--

In this section, numerical examples are present to show the effect of the length parameter on the elastic microcylinder in Figurs. 3 to 8 based on the information in Table 2. In all calculations and for simplicity, we consider $l = l_1 = l_2$. Also, in order to make the numerical results dimensionless, we divide the force stresses by P_i [29] and the Coupling stresses by $(\lambda + 2\mu)r_i$ [30]. The radial, hoop, and dimensionless shear stress distributions along the radius of the micro-cylinder are evaluated for several values of the characteristic length parameter. Corresponding solutions obtained from classical elasticity theory are also given in the figures for reference and comparison purposes. Figures 3 and 4 present the distributions of dimensionless radial and hoop stresses for a homogeneous cylinder as functions of the dimensionless radial coordinate. In these figures, the responses predicted by the micropolar elasticity theory for characteristic length parameter (l) values of $l = 0.1\mu m, 0.2\mu m, 0.3\mu m, 0.5\mu m$ are illustrated and compared with those obtained from the classical elasticity model ($l = 0$). Results indicate that the material length parameter has a significant effect on the stress distribution in the micro-cylinder. For example, a decrease in the material length parameter leads to a gradual approach towards the classical elasticity solution for the radial and hoop stresses. A rise in the characteristic length parameter leads to a significant decrease in the values of the maximum radial and tangential stresses. For example, a rise in the characteristic length parameter from $l = 0$ to $l = 0.5\mu m$ eads to a reduction of about 46% and 45% in the value of the maximum radial and tangential stresses, respectively.

Furthermore, the discrepancybetween the calculated values of stress based on the micropolar elasticity model and corresponding values based on classical elasticity is larger for the inner radius of the cylinder than for its outer radius. Moreover, the difference between the two stress predictions according to micropolar and classical elasticity theories is greater for the inner surface of the cylinder rather than for the outer one. For instance, at the inner radius, the maximum dimensionless tangential stress as predicted by the micropolar theory with $l = 0.5\mu m$ differs about 45% from that obtained by using classical elasticity, whereas this difference is reduced to approximately 5% at the outer radius. We can notice that, in the case of radial stress, the area under the stress-radius curves predicted by classical elasticity and micropolar elasticity differs by 14.9%, 32.7%, 44.5%, and 73.8% for the characteristic length parameters $l = 0.1$, $l = 0.2$, $l = 0.3$ and.$l = 0.5$

In radial stress diagram, the difference of the area under the classical theory of elasticity diagram with the micropolar theory of elasticity is equal to 8.5, 16.1, 28.6, and 45.9 respectively for the characteristic values $l = 0.1$, $l = 0.2$, $l = 0.3$ and.$l = 0.5$.

10.57647/jsm.2025.1704.13

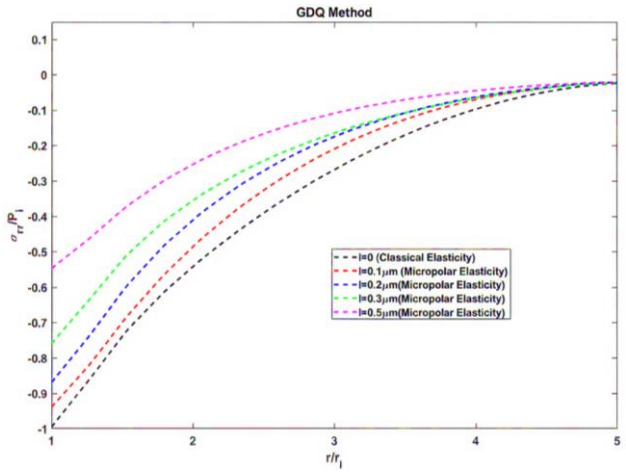

Figure 3. Radial stress distribution σ_{rr} in micropolar theory for different characteristic lengths and classical elasticity

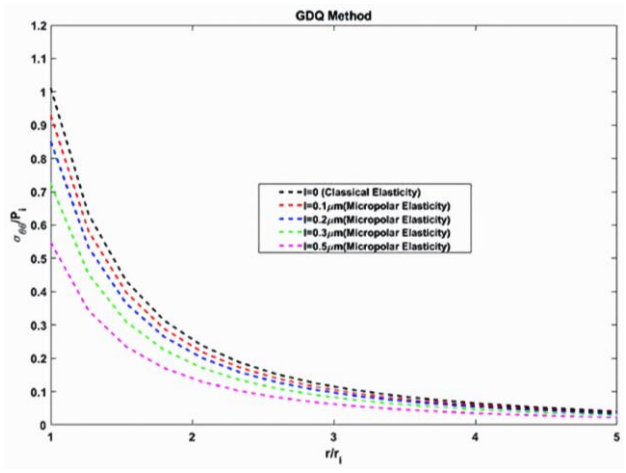

Figure 4. Hoop stress distribution $\sigma_{\theta\theta}$ in micropolar theory for different characteristic lengths and classical elasticity

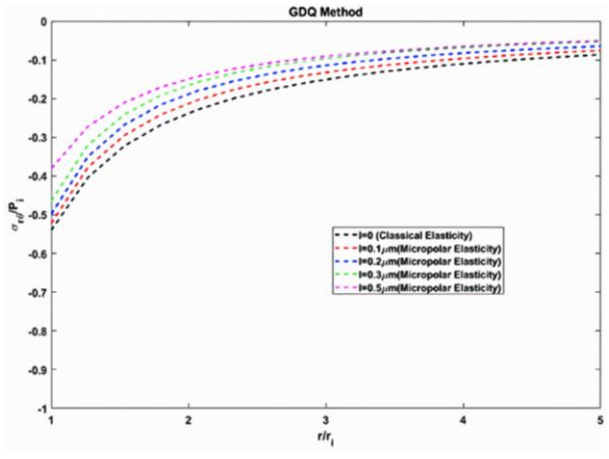

Figure 5. Shear stress distribution $\sigma_{r\theta}$ in micropolar theory for different characteristic lengths and classical elasticity

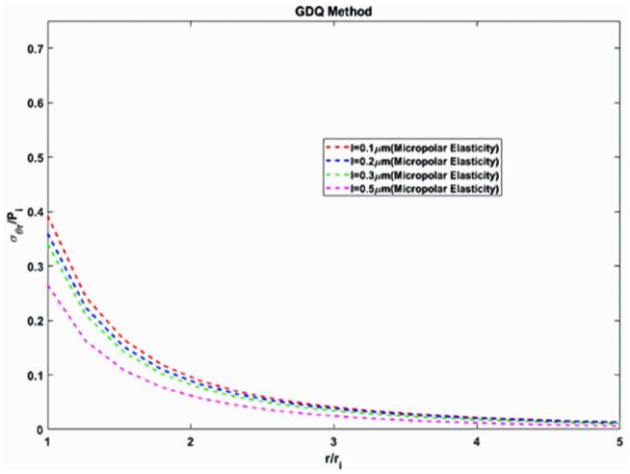

Figure 6. Shear stress distribution $\sigma_{\theta r}$ in micropolar theory for different characteristic lengths

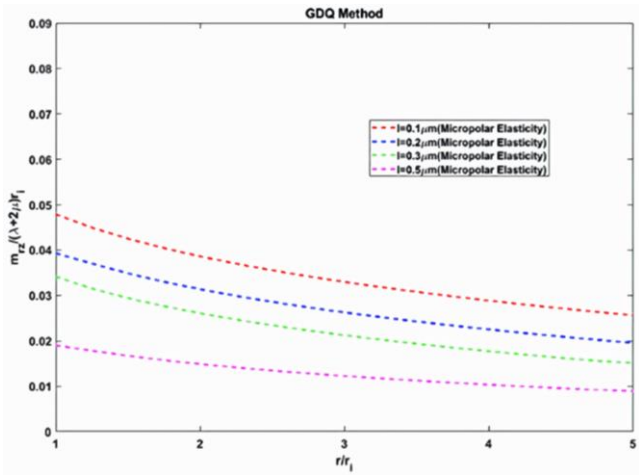

Figure 7. Couple stress distribution m_{rz} in micropolar theory for different characteristic lengths

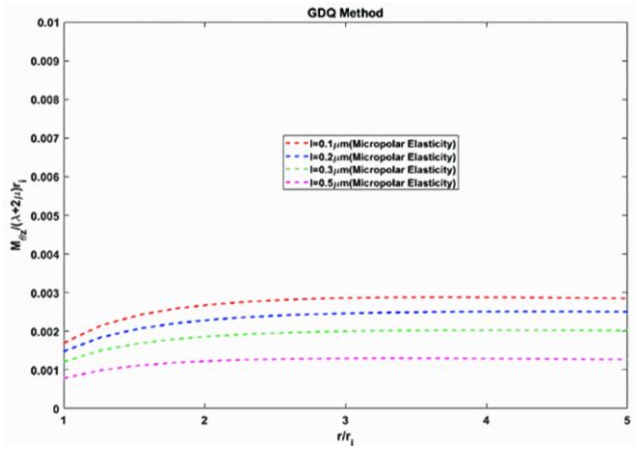

Figure 8. Couple stress distribution $m_{\theta z}$ in micropolar theory for different characteristic lengths

Figure 5 presents the variation of the dimensionless shear stress $\sigma_{r\theta}$ versus dimensionless radial coordinate for a homogeneous cylinder. In this figure, results that are obtained using the micropolar elasticity theory by taking several values of the characteristic length parameter (l) are plotted and compared to those corresponding to the classical elasticity model ($l = 0$). he numerical results clearly demonstrate that the characteristic length

10.57647/jsm.2025.1704.13

parameter has a strong influence on the shear stress distribution in the microcylinder. As its value is decreased, the response of the shear stress approaches that obtained by the classical elasticity. On the other hand, the maximum value of the shear stress $\sigma_{r\theta}$ decreases with increasing characteristic length parameter. For example, the increase in the characteristic length parameter from $l = 0$ to $l = 0.5\mu m$ decreases the calculated maximum value of the shear stress approximately by 15%. Furthermore, the difference between the values of the shear stress given by the micropolar elasticity formulation and those computed using classical elasticity is much greater in the inner radius region of the cylinder than in the outer radius region.

Besides, the areas under the radial stress distributions predicted by the classical and micropolar elasticity theories reveal differences of 9.2%, 18.7%, 28.4%, and 57.4% for the characteristic length parameter values of $l = 0.1, l = 0.2, l = 0.3$ and $l = 0.5$, respectively. Figure 6 shows the distribution of the dimensionless shear stress $\sigma_{\theta r}$ for the homogeneous cylinder as a function of the dimensionless radial coordinate as obtained from the micropolar elasticity theory for a few different values of the characteristic length parameter (l). Because this shear stress component appears only within the framework of micropolar elasticity, no corresponding results from the classical elasticity theory are available for comparison. Numerical results show that the characteristic length parameter has a significant effect on the dimensionless shear stress distribution in the micro-cylinder, especially the peak value. It can be observed that this peak will be reduced by increasing the characteristic length parameter value. As an example, it can be seen that using the characteristic length parameter from $l = 0$ to $l = 0.5\mu m$ decreases the calculated maximum shear stress by about 15%. Also, the shear stress values obtained from the micropolar elasticity model vary more considerably in the neighborhood of the inner radius than at the outer one. It is also noticed that the magnitude of the shear stress at the inner radius depicted in Figure 6 is smaller compared to the corresponding shear stress values indicated in Figure 5. Figure 7 shows the variation of the couple stress m_{rz} in the hollow micro-cylinder for different values of the characteristic length parameter. Since this component of the stress exists only in micropolar elasticity, there are no results available to compare with the values from classical elasticity theory. The results amplify the importance of the characteristic length parameter in influencing the results of the couple stress. Specifically, the results show that as the characteristic length parameter is raised, the couple stress m_{rz} also decreases. For example, raising the characteristic length parameter from $l = 0$ to $l = 0.5\mu m$ results in a decrease of about 30% in the results for the couple stress m_{rz}. Also, the difference between the maximum values of the couple stress at the inner and outer radii of the cylinder is still small. Figure 8 presents the distribution of the couple stress $m_{\theta z}$ in the hollow micro-cylinder for different values of the characteristic length parameter. Since this stress component exists only within the framework of micropolar elasticity, no comparison with the classical elasticity theory is possible. The results show that the material characteristic length parameter significantly affects the distribution of couple stress $m_{\theta z}$ in the micro-cylinder. In particular, increasing the characteristic length parameter of the material reduces the maximum magnitude of the couple stress. For example, increasing the characteristic length parameter from $l = 0$ to $l = 0.5\mu m$ decreases the maximum couple stress by about 10%. Second, the shear stress values computed at the inner and outer radii of the cylinder show a relatively small difference. However, the numerical results from the micropolar elasticity theory show that this difference is slightly larger near the outer radius than near the inner radius. Overall, the results obtained from the micropolar elasticity formulation confirm that the characteristic length parameter plays an important role in the stress response of micro-cylinders and increasing this parameter results in the reduction of the maximum value of force and couple stresses.

4.1. Verification of the exact solution with the numerical method (GDQ Method)

Two exact solution methods and the GDQ numerical method were plotted to compare the radial stress distribution for the specified characteristic length (Figure 9). Table 2 was used to validate this verification. From the plot (Figure 9) it can be seen that the results obtained from the two theories agree well with each other.

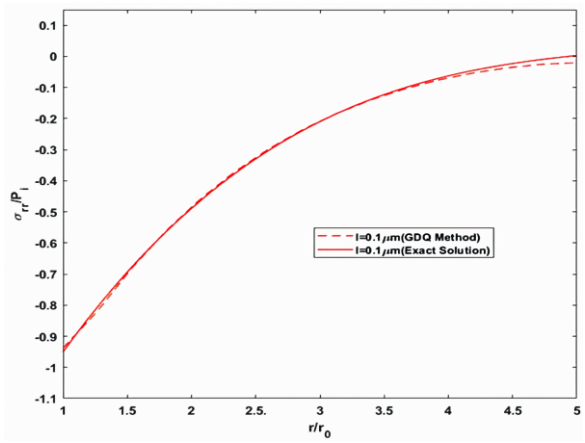

Figure 9. Comparison of the exact solution and numerical method for σ_{rr} at a given characteristic length parameter

10.57647/jsm.2025.1704.13

5. Conclusion

In the present study, the length-scale-dependent stress response of a hollow cylinder was fully investigated within the framework of micropolar elasticity. The formulation of the governing field equations in polar coordinates, incorporating size effects through characteristic length parameters, and were efficiently solved using the Generalized Differential Quadrature (GDQ) method. Moreover, a systematic parametric analysis has been performed to quantify the influence of the characteristic length parameter on the resulting distributions of interest.

The main conclusions of the present analysis are summarized below:

The material's characteristic length parameter significantly influences the mechanical response of the micro-cylinder.

As this parameter decreases, the results from micropolar theory asymptotically converge towards the predictions of classical elasticity, thereby validating the presented model and solution methodology.

The increase in the characteristic length parameter leads to a remarkable reduction in the peak values of the radial, hoop, and shear stress components. More precisely, by increasing the characteristic length parameter from l=0 to l=0.5μm, the maximum values of radial and hoop stresses have been reduced about 46% and 45%, respectively. This stress reduction can be attributed to the ability of micropolar theory to account for stiffening effects arising from the material's internal microstructure.

Micropolar effects are more pronounced at the inner radius of the cylinder compared to the outer radius. This phenomenon is justified by the higher stress gradient near the inner surface of a pressurized hollow cylinder, where rapid variations in the stress field accentuate the small-scale size effects.

The distribution of couple stresses, which appear exclusively in micropolar theory, also showed a strong dependence on the characteristic length parameter. Increasing this parameter significantly reduces the magnitude of the couple stresses.

The GDQ method proved to be an efficient and accurate numerical tool for solving the associated high-order differential governing equations and complex boundary conditions.

As shown in Table 2 and also in Eqs. (21), the cylinder is subjected only to internal pressure (10 MPa) and the external pressure is zero. Also, Figure 3 shows that at the inner radius, the difference between the stress curve in classical theory for $l = 0$ and the curves corresponding to various values of l in micropolar theory is quite noticeable. In other words, as l increases, according to micropolar theory, the stress value should decrease, and as one moves toward the outer radius, these curves approach each other and eventually nearly coincide at the outer radius. The novelty of the present manuscript is attributed to regenerate ability of the difference governing equations with respect to the change of the number of the domain grid points. This is required for stabilizing the numerical method by finding appropriate number of the grid points. The GDQ method is just used for discretizing the differential equations. Some other methods such as finite element or volume might also have been applied. The regenerate ability of the difference equations is a base on top of which the assembling of the difference equations can be fulfilled. The regenerate ability is achieved by extracting the grid point indices from the terms of the differential equations and sending them to the coefficients thereof. This is considered as one novelty of the current manuscript. In conclusion, this study unequivocally demonstrates that for the accurate design and analysis of cylindrical structures at micro and nano scales (such as MEMS components, advanced composite shells, and engineered materials), the use of generalized continuum theories like micropolar elasticity, which can incorporate length scale effects, is essential. Neglecting these effects can lead to inaccurate predictions and, consequently, sub-optimal design. For future work, this research can be extended by considering more complex conditions such as functionally graded materials (FGMs), thermo-mechanical loadings, dynamic analyses, and the investigation of shell structures with more general geometries.

Authors Contribution

A.K.A. developed the theoretical formulation and performed the numerical simulations. M.J. supervised the research, contributed to the formulation and interpretation of the results, and revised the manuscript. S.M.K. contributed to the problem definition, discussion of the numerical results, and editing of the manuscript. All authors read and approved the final manuscript

Availability of data and materials

The datasets generated and/or analyzed during the current study are available from the corresponding author on reasonable request.

Conflict of interests

The authors declare no conflicts of interest.

References

[1] Eremeyev, V. A., Lebedev, L. P., & Altenbach, H. Mechanics of Micropolar Continua: A Review from Foundations to Applications. ZAMM - Journal of Applied Mathematics and Mechanics. (2022). DOI: https://doi.org/10.1002/zamm.202100391

[2] Lakes, R. S. Micropolar Elasticity: A Brief Review. Journal of Elasticity. (2022). DOI: https://doi.org/10.1007/s10659-022-09910-7

[3] Biswas, P., & Poh, L. H. On the role of microstructure length scale in the plastic response of the micropolar continuum. International Journal of Solids and Structures. (2022). DOI: https://doi.org/10.1016/j.ijsolstr.2022.111698

[4] Thai, C. H., Ferreira, A. J. M., & Phung-Van, P. Size-dependent behavior of functionally graded micropolar plates. Composite Structures. (2021). DOI:https://doi.org/10.1016/j.compstruct.2021.114266

[5] Nejad, M. Z., Jabbari, M., & Ghannad, M. Elastic analysis of functionally graded rotating thick-walled cylindrical shell under pressure with micropolar model. Journal of Mechanics of Materials and Structures. (2017). DOI: https://doi.org/10.2140/jomms.2017.12.489

[6] Ghorbani, A., Ghorbani, A., & Mohammadi, M. Thermoelastic analysis of a functionally graded micropolar cylindrical shell. Mechanics Based Design of Structures and Machines. (2023). DOI:https://doi.org/10.1080/15397734.2023.2176745

[7] Kumar, R., & Sharma, K. D. Wave propagation in a micropolar cylindrical porous media. Mathematics and Mechanics of Solids. (2021). DOI: https://doi.org/10.1177/10812865211022561

[8] Shu, C. Differential Quadrature and Its Application in Engineering. Springer-Verlag, London, (2000). DOI: https://doi.org/10.1007/978-1-4471-0407-0

[9] Tornabene, F., Fantuzzi, N., & Bacciocchi, M. The GDQ Method for the Free Vibration Analysis of Arbitrarily Shaped Laminated Composite Shells Using a NURBS-Based Isogeometric Approach. Composite Structures, 154, 190-218, (2016). DOI:https://doi.org/10.1016/J.COMPSTRUCT.2016.07.041

[10] Bellman, R., Kashef, B.G, Casti, J. " Differential quadrature: a technique for the rapid solution of nonlinear partial differential equations". J. of Computational Physics, v10, pp. 40–52, (1972). DOI: https://doi.org/10.1016/0021-9991(72)90089-7

[11] Quan, J.R., Chang, C.T. "New insights in solving distributed system equations by the quadrature method – I Analysis". Computers and Chemical Engineering, v13, pp. 779-788, (1989). DOI: https://doi.org/10.1016/0098-1354(89)85051-3

[12] Shu, C., Richards, B.E. "Application of generalized differential quadrature to solve two-dimensional incompressible Navier-Stokes equations". Int. J. of Numerical Methods in Fluids, v15, pp. 791- 798, (1992). DOI: https://doi.org/10.1002/FLD.1650150704

[13] Shishesaz, M., Zakipour, A., Jafarzadeh, A. "Magneto-elastic analysis of an annular FGM plate based on classical plate theory using GDQ method". Latin American Journal of Solids and Structures, pp. 2736-2762, (2016). DOI: https://doi.org/10.1590/1679-78252880

[14] Panah, M., Khorshidvand, A.R., Khorsandijou, S.M., Jabbari, M. "Axisymmetric nonlinear behavior of functionally graded saturated poroelastic circular plates under thermo-mechanical loading". Proc IMechE Part C: J Mechanical Engineering Science,0(0), pp.1–23, (2021). DOI: https://doi.org/10.1177/09544062211051684

[15] rezaei, m., khorshidvand, a.r., khorsandijou, s.m., jabbari, m. "influence of length scale parameter on nonlinear bending of functionally graded saturated porous rectangular microplates". special topics & reviews in porous media an International Journal, 13(2), pp.1–40, (2022). DOI:https://doi.org/10.1615/SpecialTopicsRevPorousMedia.2022040711

[16] Wu, T.Y., Wang, Y.Y., Liu, G.R. " Free vibration analysis of circular plates using generalized differential quadrature rule". Comput. Methods Appl. Mech. Engrg.,191, pp.5365–5380, (2002). DOI: https://doi.org/10.1016/S0045-7825(02)00463-2

[17] Tornabene, F., Viola, E. " Vibration analysis of spherical structural elements using the GDQ method". Computers and Mathematics with Applications, 53, pp. 1538–1560, (2007). DOI: https://doi.org/10.1016/j.camwa.2006.03.039

[18] Brischetto, S., Tornabene, F., Fantuzzi, N. Viola. E. " 3D Exact and 2D Generalized Differential Quadrature Models for Free vibration analysis of functionally graded plates and cylinders". Meccanica, 51(9), pp.2059-2098, (2016). DOI: https://doi.org/10.1007/S11012-016-0361-Y

[19] Alinaghizadeh, F., Shariati, M. "geometrically non-linear bending analysis of thick two-directional functionally graded annular sector and rectangular plates with variable thickness resting on non-linear elastic foundation". Composites Part B, 86, pp.61-83, (2016). DOI:https://doi.org/10.1016/J.COMPOSITESB.2015.05.010

[20] Barati, A., Norouzi, S. "Nonlocal elasticity theory for static torsion of the bi-directional functionally graded microtube under magnetic field". JCAMECH, 51(1), pp. 30-36, (2020).

DOI:https://doi.org/10.22059/JCAMECH.2019.294263.462

[21] Mohammadi, A., Lashini, H., Habibi, M., H. Safarpour, H. "Influence of Viscoelastic Foundation on Dynamic Behavior of the Double Walled Cylindrical Inhomogeneous Micro Shell Using MCST and with the Aid of GDQM". Journal of Solid Mechanics, 11(2), pp. 440-453, (2019).
DOI: https://doi.org/10.22034/JSM.2019.665264

[22] V. Kaliraman , R.K. Poonia, " Elastic Wave Propagation at Imperfect Boundary of Micropolar Elastic Solid and Fluid Saturated Porous Solid Half-Space ", Journal of Solid Mechanics Vol. 10, No. 3 pp. 655-671, (2018).
https://sanad.iau.ir/Journal/jsm/Article/909269

[23] Kumar R., Chawla V., "Effect of rotation and stiffness on surface wave propagation in elastic layer lying over a generalized thermo-diffusive elastic half-space with imperfect boundary", Journal of Solid Mechanics 2(1): 28-42, (2010).
https://journals.iau.ir/article_514354_5611efd0659aa849e2c3d0d9c8d4c2ba.pdf

[24] Kumari N., "Reflection and transmission of longitudinal wave at micro polar viscoelastic solid/fluid saturated incompressible porous solid interface", Journal of Solid Mechanics 6(3): 240-254, (2014).
https://sanad.iau.ir/fa/Article/909086?FullText=FullText

[25] Dehbani., Jabbari, M., Khorshidvand, A.R., Javadi, M.," Analytical solution of micropolar functionally graded materials (FGM) hollow cylinder under thermal asymmetric load (r, θ)." ZAMM-Journal of Applied Mathematics and Mechanics,102,2, (2021).
DOI: https://doi.org/10.1002/zamm.202000156

[26] Dehbani., Jabbari, M., Khorshidvand, A.R., Javadi, M.," Two-dimensional analytical solution of micropolar magneto-thermoelasticity FGM hollow cylinder under asymmetric load (r, θ)." Physica Scripta, 96, 12, (2021).
DOI: https://doi.org/10.1088/1402-4896/ac3313

[27] Sadd, M. H. "Elasticity: Theory, Applications, and Numerics". Oxford: Elsevier Academic Press, (2005).
https://www.inspectioncopy.elsevier.com/book/details/9780443132452

[28] Chu, L., Dui, G." Exact solutions for functionally graded micro-cylinders in first gradient elasticity." International Journal of Mechanical Sciences, 148, pp. 366–373, (2018).
DOI:https://doi.org/10.1016/J.IJMECSCI.2018.09.011

[29] Chu, L., Dui, G. "Exact solutions for functionally graded micro-cylinders in first gradient elasticity". International Journal of Mechanical Sciences, 148, 366–373, (2018).
DOI:https://doi.org/10.1016/J.IJMECSCI.2018.09.011

[30] Collin, F., Caillerie, D., Chambon, R. "Analytical solutions for the thick-walled cylinder problem modeled with an isotropic elastic second gradient constitutive equation". International Journal of Solids and Structures, 46, 3927–3937, (2009).
DOI:https://doi.org/10.1016/J.IJSOLSTR.2009.05.017